Simulations of the dynamics at an RNA–protein interface

Thomas Hermann[1,2] and Eric Westhof[1]

[1]*Institut de Biologie Moléculaire et Cellulaire du CNRS, UPR 9002, Equipe de Modélisation et Simulation des Acides Nucléiques, 15 rue René Descartes, F-67084 Strasbourg, France.* [2]*Present address: Memorial Sloan-Kettering Cancer Center, Cellular Biochemistry and Biophysics Program, Box 557, 1275 York Avenue, New York, New York 10021, USA*

Molecular dynamics simulations of the RNA-binding domain of the U1A spliceosomal protein in complex with its cognate RNA hairpin, performed at low and high ionic strength in aqueous solution, suggest a pathway for complex dissociation. First, cations condense around the RNA and compete with the protein for binding sites. Then solvated ions specifically destabilize residues at the RNA–protein interface. For a discrete cluster of residues at the complex interface, the simulations reveal an increased deviation from the crystal structure at high salt concentrations while the remaining protein scaffold is stabilized under these conditions. The microscopic picture of salt influence on the complex suggests guidelines for rational design of interface inhibitors targeted at RNA–protein complexes.

The strong influence of ions on the stability of RNA–protein complexes is due to electrostatic interactions that play central roles in the formation of ion pairs or hydrogen bonds between charged groups[1]. On the macroscopic scale, the thermodynamic and kinetic effects of ions on the stability of protein–nucleic acid complexes have been extensively studied[2,3]. In contrast, the underlying molecular mechanisms of salt-induced complex destabilization are not well described. We have performed molecular dynamics (MD) simulations in aqueous solution to study the dynamics of intermolecular interactions in an RNA-complex of the RNA-binding domain of the U1A protein in the presence of low and high concentrations of monovalent salt.

The U1A protein participates in pre-mRNA splicing[1,4]. An N-terminal RNA-binding domain comprising the RNP1 and RNP2 motifs, highly conserved among many RNA-binding proteins[5], is responsible for binding of the U1A protein to its target hairpin structure in U1 small nuclear RNA (Fig. 1*a*)[6]. The complex stability of U1A bound to RNA depends strongly on the presence of salt. The dissociation constant for the complex increases by five orders of magnitude when the concentration of monovalent salt is raised from 250 mM to 1M NaCl[7]. Here, we investigate molecular dynamics of the RNA–protein interface during a simulated 'salt jump' in which a concentrated solution of salt is allowed to rapidly mix with a buffer containing the U1A–RNA complex pre-formed under low ionic-strength conditions.

Molecular dynamics simulations at 100 mM and 1 M NaCl

Simulations were performed in explicitly treated aqueous solvent prepared by equilibrating randomly placed water molecules around the crystal structure of the RNA-binding domain of U1A protein complexed with an RNA hairpin[8]. Monovalent salt was treated by adding Na^+ and Cl^- ions. For the simulations at 1 M salt, ions were initially packed at the periphery of the solvent box. This shell of salt was dissolved during the MD simulations. Thermal motion of the solvent molecules was sufficient to evenly redistribute the ions throughout the box, attested by the short-range structure of the NaCl solution (Fig. 1*b*,*c*).

High-affinity sites for ions

In the 1 M salt simulations, a high density of Na^+ ions was observed in proximity to the RNA (Fig. 1*c*) corresponding to the

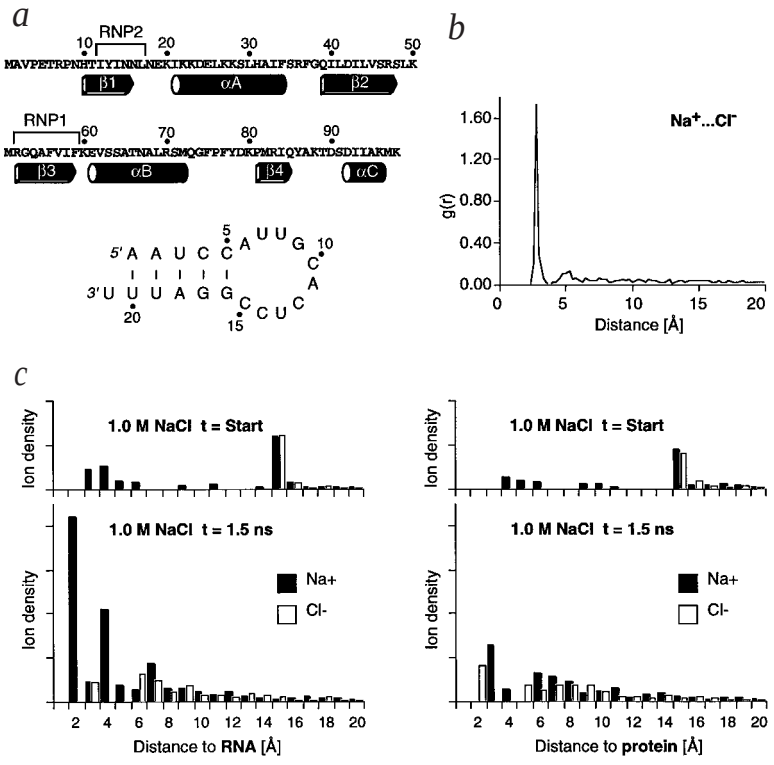

Fig. 1 The U1A protein/RNA/solvent system used in molecular dynamics (MD) simulations of an *in silico* salt-jump experiment. ***a***, Sequence and secondary structure elements of the RNA-binding domain of the U1A protein and its cognate 21 nt RNA hairpin[8,11]. The protein secondary structure as revealed by crystal structure analysis[8] is indicated below the sequence. Cylinders depict α-helices, αA–αC, and arrows depict β-strands, β1–β4. The positions of conserved RNA-binding motifs RNP1 and RNP2 are marked. ***b***, Inter-ionic radial distribution function g(r) of NaCl calculated after 0.1 ns of productive MD calculation in which the salt was dissolved in the solvent box to give a solution of 1.0 M concentration. The two peaks at ~2.8 Å and ~5.0 Å indicate, respectively, contact ion pairs and ions separated by one shell of hydration water, in accord with previous studies on aqueous NaCl solutions[23,24]. ***c***, Density distributions of ions around the solute RNA (left) and protein (right), calculated for the starting configuration (top) and after 1.5 ns of simulation (bottom), reveal that the ions diffused from their initial positions at the periphery of the box and distributed into the bulk solvent. The large imbalance between the distributions of cations and anions in proximity of the RNA (bottom, left) shows how Na^+ ions accumulate around the nucleic acid and at the same time anions are excluded from its close neighborhood. In contrast, the densities of both anions and cations are roughly in equilibrium around the protein (bottom, right). Density values in all four panels are drawn to the same scale. Quantitatively similar distributions after 1.5 ns were obtained for the simulations at 0.1 M NaCl, however, due to the smaller number of ions present, the absolute density values were smaller (data not shown).

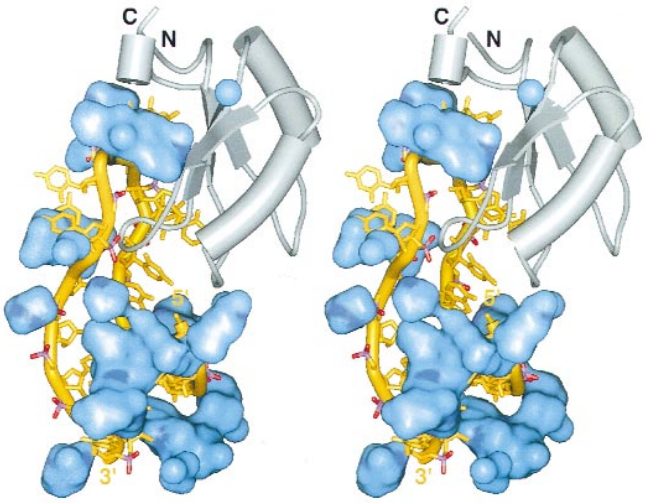

Fig. 2 Stereo view of high-occupancy sites for Na^+ ions (blue surface), observed during an MD simulation of the U1A–RNA complex at 1 M NaCl concentration. Protein β-strands are shown as arrows, α-helices as cylinders, RNA as backbone tube and base sticks (orange). High-occupancy sites for Na^+ ions were calculated by integrating over volume elements occupied by ions within the solvent box for coordinate sets spatially aligned by least-squares fitting on the RNA–protein complex, extracted at intervals of 5 ps over the last 100 ps of the 1.55 ns trajectory. Darker shading of blue indicates higher Na^+ densities. No additional high-occupancy sites were found beyond those due to neutralization of the RNA backbone.

long-known condensation of counterions around polyions[9]. Integration of the spatial distribution of ions over the MD trajectories revealed high-affinity regions for cations located exclusively at the RNA (Fig. 2). Calculations of high-occupancy Na^+ sites, performed for consecutive segments of the trajectories, demonstrate that the accumulation of Na^+ around the RNA is fast, occurring early during the simulations. However, cation accumulation in proximity of the RNA is a statistical process: not instantaneous but time-averaged high-density values mark regions preferred by Na^+ ions. As seen before by NMR[10], during the simulations the solvated Na^+ ions are mobile and do not undergo dehydration even at high-occupancy sites. The highest densities of cations were observed around the termini of the RNA, where the β_2-β_3 loop of U1A protrudes through the RNA loop, and where the protein C-terminus contacts the RNA. For the Cl^- co-ions, only a single high-affinity site was observed at the side chain of Arg 83 and the U 8 base of the RNA. The anion density in proximity of the RNA was lower as compared to the bulk solvent (Fig. 1*c*), an effect described as co-ion exclusion in earlier model calculations on double-stranded DNA[2].

Salt destabilizes the RNA component

The overall structure of the RNA–protein complex remained stable during the simulation at low salt concentration. The root mean square (r.m.s.) deviation from the crystal structure, calculated separately for the protein and the RNA, reached a stable plateau, oscillating around 1.5 Å for both components (Fig. 3*a*). At high salt concentration, a similar trend was observed for the protein, while the RNA behaved very differently (Fig. 3*a*). In two independently calculated trajectories, the r.m.s. deviation of the RNA continuously rose until the end. Thus, as observed macroscopically[2,3], we find, on the microscopic scale of the simulations, that high concentrations of salt exert their destabilizing effect primarily on the nucleic acid component in the RNA–protein complex.

In order to analyze molecular details of the salt-induced destabilization, we calculated thermal B-factors and r.m.s. deviations separately for each residue. The B-factors reflect the fast dynamics of the complex on the short time scale of the simulations. The r.m.s. deviations per residue reveal the evolution of the complex structure from local distortions of the starting coordinates in the crystal towards rearrangements governing the conformational dynamics beyond the scale of the calculations.

B-factors reveal high stability of the conserved RNP domain

The B-factors calculated from the simulation at 100 mM NaCl concentration are in good agreement (data not shown) with the reported experimental values[8]. A remarkable difference in the influence of salt on the short-scale dynamics between the conserved RNP motifs and the rest of the protein is observed when

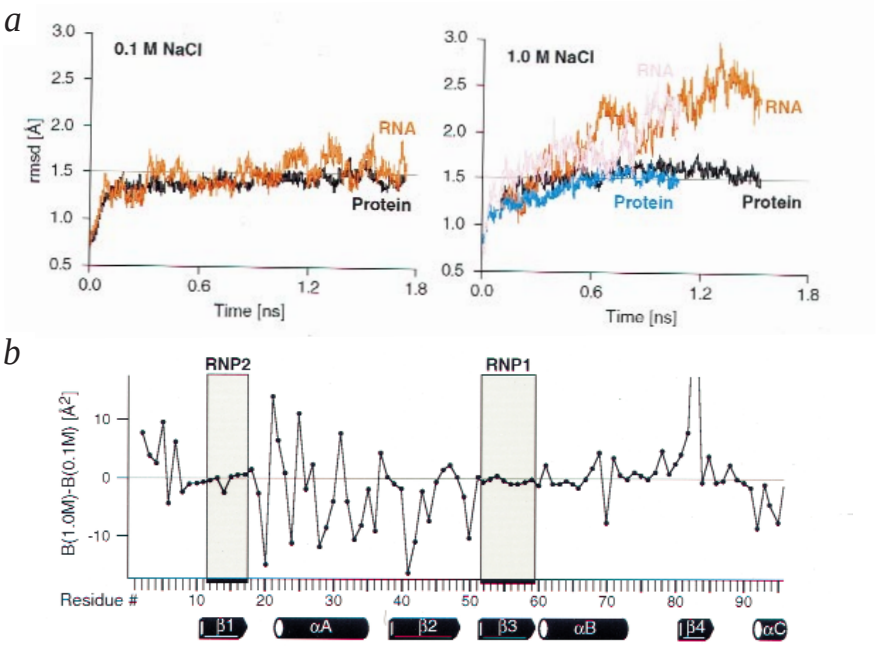

Fig. 3 Dynamic flexibility of the U1A protein and RNA hairpin components of the complex. ***a***, Root mean square (r.m.s.) deviations of the structures of the protein (black) and the RNA (red) from the crystal structure recorded over the time course of the MD simulations at NaCl concentrations of 0.1 M (left) and 1.0 M (right). The r.m.s. deviations from a second independent trajectory calculated at 1.0 M NaCl are drawn in blue and magenta. ***b,*** Differences between the per-residue B-factors of the U1A protein in the MD simulations at 1.0 M and 0.1 M NaCl concentration. B-factors were calculated from data of the 1.0-1.5 ns time window of the MD simulations. Secondary structure elements, as observed in the crystal[8], and the positions of the conserved RNA-binding motifs RNP1 and RNP2 are indicated at the bottom.

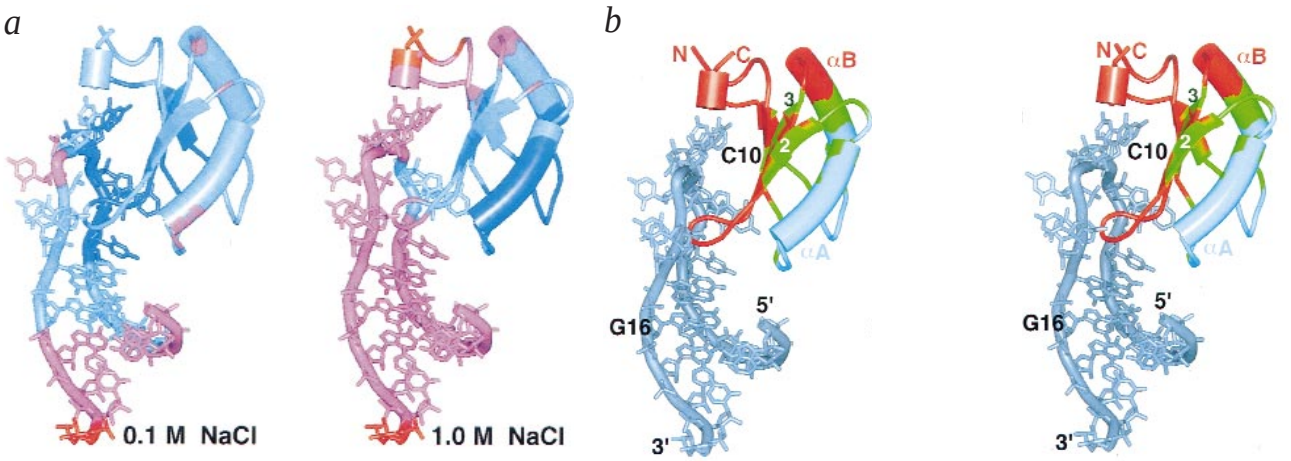

Fig. 4 Structural stability of the U1A–RNA complex during the MD simulations. ***a***, Deviation of residues from the crystal structure observed at 0.1 M (left) and 1.0 M (right) NaCl concentration. Red colors indicate high, blue colors low deviations. ***b***, Stereo view of the differential map indicating regions destabilized in high salt (red), regions stabilized in high salt (blue) and regions showing stability indifferent to salt (green).

the difference of per residue B-factors between the simulations at high and low NaCl concentrations is plotted (Fig. 3*b*). The dynamics of residues within the RNP motifs is not significantly affected by the salt concentration while outside the conserved regions a strong dependence of residue flexibility on the ionic strength is observed. Experimentally, these are regions with high B-factors in crystal structures of the protein in the absence of RNA[11]. This suggests that interactions of the highly conserved RNP motifs are predominantly hydrophobic, for example, the stacking of side chains within the protein and intermolecular interactions with RNA bases. In RNA-binding proteins containing the RNP motif, three aromatic amino acids, involved in the stacking interactions with bases, are conserved[5]. In contrast to the polar hydrogen bonds, the intermolecular stacking contacts are not affected by the presence of high salt concentrations, attested by their stable persistence in the simulations at 1 M NaCl (data not shown). A dramatic difference of B-factors between low and high salt concentrations is found for Arg 83, which is involved in the only high-occupancy site for Cl^- ions observed in the simulations at 1 M NaCl.

Deviations from the crystal structure

In the presence of 100 mM NaCl, the RNA–protein interface comprising the β-sheet, the β_2-β_3 loop, along with the C-terminus of the protein and the nucleotides U7–A11 of the RNA display the lowest deviations from the crystal structure (Fig. 4*a*). Regions of high deviations under these conditions were the unpaired U13 and the termini of the RNA, outside the binding interface. In contrast, in the simulations at 1 M NaCl, high deviations from the crystal structure were observed for almost all RNA residues as well as for both the β_2-β_3 loop and the C-terminus of the protein that forms most of the polar hydrogen bonds to the RNA (Fig. 4*a*). Thus, the destabilizing influence of salt on the RNA–protein complex is exhibited predominantly on the RNA component and on residues of the protein that make up the polar RNA-binding surface.

The dynamic nature of the single-stranded loop of the RNA and the C-terminus of U1A changes extensively upon formation of the RNA–protein complex. This results in the ordering of nucleotides within the RNA loop and an induced-fit type docking of helix αC which exposes the hydrophobic surface of the RNP motifs[12]. The principle of microscopic reversibility suggests that the salt-induced distortion of the RNA–protein interface observed in the simulations at high salt concentrations may represent the initial phase of the dissociation of the components.

In the absence of observed direct contacts between the ions to either protein or RNA, the influence of salt on the stability of the complex is exerted by both long-ranging electrostatic interactions with the RNA and reorganization of solvent molecules around the solute. Due to the high local concentration of cations around the RNA, a competition for water molecules occurs at the surface of the complex between the equilibria for the solvation of the protein–RNA complex and the salt ions (Fig. 5*a*).

Residues within helix αB displayed the lowest deviations from the crystal structure in the simulations at both ionic strengths. The structure of helix αA was retained to an even higher degree in the calculations at 1 M NaCl as compared to the low salt simulations, suggesting a localized salt-induced stabilization. The differential effects of monovalent salt on the structural stability of different domains of the U1A protein becomes evident when the differences in per residue r.m.s. deviations between low and high salt conditions are compared (Fig. 4*b*). The protein divides into two distinct regions with different responses to ionic strength, namely the RNA-binding region that is destabilized by salt and the part containing helix αA and neighboring residues for which salt-induced stabilization is observed.

Details of salt-induced complex destabilization

The destabilization of the RNA–protein interface by a high concentration of NaCl is reflected by the fluctuating behavior of key intermolecular hydrogen bonds (Fig. 5*b*). The hydrogen bond between Arg 52 and G16 of the conserved C5–G16 base pair, which plays an important role in binding and positioning the RNA on the protein[8,12], is repeatedly breaking and re-forming during the simulations at high salt while it is stable under low-salt conditions. Similar fluctuations are observed for the hydrogen bond between Gln 85 and C10 that is a conserved identity element of the U1 RNA. Mutation of the C to U at this position strongly reduces binding to the U1A protein[13]. Of all the nucleotides, C10 displays the lowest deviations from the crystal structure during the simulation at low-salt while it is among the most mobile residues under high-salt conditions. Around the

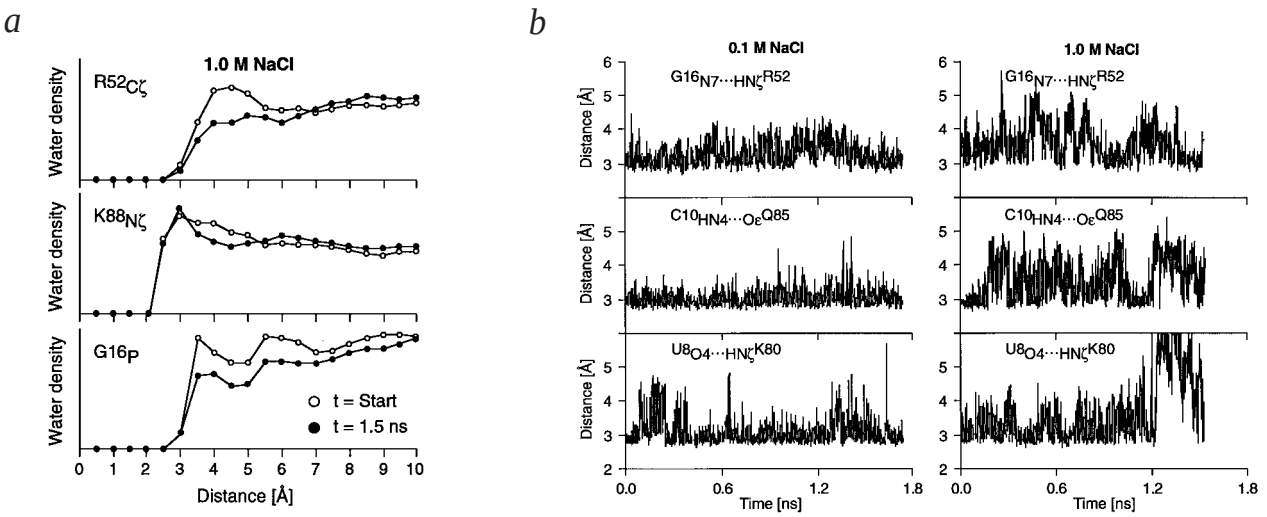

Fig. 5 Microscopic effects of 1.0 M NaCl on protein–RNA complex structure and solvation during the MD simulations. ***a***, Density of water molecules around selected charged groups that are involved in intermolecular interactions[8]. Competition for water molecules between the hydration equilibria of the RNA/protein components and the ions at the surface of the complex is attested by the water density which, during the simulations, decreases around charged groups. At the start of the calculation (open circles), the NaCl is packed at the periphery of the solvent box, away from the RNA–protein complex, and the water density around the charged groups corresponds to the situation in the absence of salt. After 1.5 ns of simulation (filled circles), the salt is distributed throughout the box and around the RNA–protein complex. Densities were calculated by counting the number of water molecules in a sphere of given radius around the indicated atoms, normalized by the sphere volume. ***b***, Stability of intermolecular hydrogen-bonds in the complex monitored for three representative examples in simulations at 0.1 M NaCl (left panels) and 1.0 M NaCl concentration (right panels). Distances between the heavy atoms of the hydrogen donor and acceptor groups are plotted. The indicated hydrogen-bonds play an important role in the architecture of the U1A–RNA complex[8].

C10 phosphate group, a high density of Na^+ ions is found throughout the simulations (Fig. 2), suggesting salt-induced structural deformations at this residue. The binding of a Cl^- anion to the neighboring Arg 83 may participate in the high-salt destabilization effect.

While at 1 M NaCl, strong fluctuations of the intermolecular hydrogen-bonds are found, only few bonds are ultimately disrupted. One example is the hydrogen bond between Lys 80 and U8 that breaks after 1.2 ns of simulation (Fig. 5*b*). Due to the short simulation time, it cannot be ruled out that disrupted contacts may be re-established. We conclude, however, that the increased dynamics of intermolecular bonds at the RNA–protein interface observed in the simulations at high ionic strength are the basis for the salt-induced dissociation of the complex. Competing interactions of the residues at the interface, either intramolecular or with the solvent, may become favorable as a consequence of the structural fluctuations ultimately leading to the dissociation of the RNA–protein complex. In the intact complex, charged groups that are involved in interactions between the RNA and the protein, may transiently become free and later be solvated by ions. On the microscopic scale, this dynamic process corresponds to the reverse of the macroscopically observed release of ions from the nucleic acid upon binding of a protein[3].

At a concentration of 1 M NaCl, the U1A protein alone is both stable and soluble, while the half-life time of the U1A–RNA complex is only 8 ms[7]. Processes in the millisecond range are still beyond the time spans accessible to MD simulations. However, simulation times of 1 ns have been sufficient to reveal the stabilizing influence of salt on the structure of a peptide[14]. While the time limitations render it unlikely to observe dissociation in a simulation of the U1A–RNA complex, the calculations presented here provide a first microscopic picture of early events in salt-induced destabilization within an RNA–protein interface. Microscopic reversibility suggests that dynamic changes leading to complex destabilization may represent the reverse of the association process when the RNA–protein complex forms from its components.

Design of interface inhibitors

The simulations presented here suggest that inhibitors targeted at protein-RNA interfaces[15,16] should combine two principal features. First, flexible cationic groups could compete with the charged protein groups for binding to the RNA, thus, destabilizing the pre-formed RNA–protein complex. Second, shape-sensitive and other non-polar contacts, such as stacking and van der Waals interactions, could anchor the drug specifically on the RNA. To overcome destabilizing effects of free ions or RNA-binding proteins on the inhibitor–RNA interaction *in vivo*, the inhibitor could either shield its salt bridges to the RNA or contain additional outlying and flexibly linked cationic groups.

Methods

MD simulations. MD simulations on the U1A–RNA complex, starting from the crystal structure[8], were performed with AMBER[17,18] at a time step of 2 fs with bonds to hydrogens fixed by SHAKE[19]. Constant temperature of 298 K and pressure of 1 atmosphere were maintained by external coupling with time constants of 0.4 ps and 0.5 ps, respectively[20]. Van der Waals interactions were truncated at 9.0 Å, while electrostatic interactions were fully calculated with the Particle Mesh Ewald method[21].

Treatment of salt. For the simulations at 0.1 M and 1.0 M NaCl, respectively, 21 Na^+/10 Cl^- and 104 Na^+/93 Cl^- ions were included in a solvent box typically containing ~6500 SPC/E water[22] molecules. The excess of Na^+ was added in order to account for the charge of the RNA–protein complex at physiological pH. At low salt concentration, the ions were placed according to the electrostatic potential such that no ion was closer than 4.5 Å to any solute atom. At 1 M NaCl, the additional ions were packed at the periphery of the solvent box, at least 15 Å away from the RNA–protein complex, at the start of the simulation.

Equilibration protocol. After 200 steps of conjugate gradient minimization on the water molecules, 50 ps of solvent equilibration at 298 K were calculated with ions free and protein/RNA fixed except for hydrogens. Followed a restart at 10 K and heating to 298 K in steps of 50 K, with 10 ps of simulation at each temperature without applying any constraints. For the simulations at low-salt conditions, the productive MD phase followed immediately. For simulations at 1 M NaCl, additional heating was performed to obtain a rapid redistribution of the ions. Therefore, the system was simulated at 900 K for 5 ps, followed by cooling to 298 K over 2 ps, with protein and RNA kept fixed in both phases.

Following equilibration, one reference trajectory of 1.75 ns at low-salt conditions and two independent trajectories of 1.55 ns and 1.10 ns, with slight differences in the heating phase, were calculated for the high-salt system. The results reported for the 1 M NaCl conditions were reproducibly observed in both high-salt trajectories.

Acknowlegments

T.H. was supported by an EMBO long-term fellowship and a DFG grant. E.W. thanks the Institut Universitaire de France for supporting grants.

Correspondence should be addressed to E.W. *email: westhof@ibmc.u-strasbg.fr*

Received 7 January, 1999; accepted 25 March, 1999.

1. Nagai, K. & Mattaj, I.W. *RNA–protein interactions*. (IRL Press, Oxford; 1994).
2. Anderson, C.F. & Record, M.T. *Annu. Rev. Phys. Chem.* **46**, 657–700 (1995).
3. Record, M.T., Zhang, W. & Anderson, C.F. *Adv. Prot. Chem.* **51**, 281–353 (1998).
4. Steitz, J.A., Black, D.L., Gerke, V., Parker, K.A., Krämer, A. *et al.* In *Structure and function of major and minor small nuclear ribonucleoprotein particles* (ed. Birnstiel, M.L.) 115–154 (Springer-Verlag, New York; 1988).
5. Nagai, K., Oubridge, C., Ito, N., Avis, J. & Evans, P.R. *Trends Biochem. Sci.* **20**, 235–240 (1995).
6. Scherly, D., Boelens, W., Van Venrooij, W.J., Dathan, N.A., Hamm, J. *et al. EMBO J.* **8**, 4163–4170 (1989).
7. Hall, K.B. & Stump, W.T. *Nucleic Acids Res.* **20**, 4283–4290 (1992).
8. Oubridge, C., Ito, N., Evans, P.R., Teo, C.-H. & Nagai, K. *Nature* **372**, 432–438 (1994).
9. Manning, G.S. *J. Chem. Phys.* **51**, 924–933 (1969).
10. Braunlin, W.H. *Adv. Biophys. Chem.* **15**, 89–139 (1995).
11. Nagai, K., Oubridge, C., Jessen, T.H., Li, J. & Evans, P.R. *Nature* **348**, 515–520 (1990).
12. Allain, F.H.-T., Gubser, C.C., Howe, P.W.A., Nagai, K., Neuhaus, D. *et al. Nature* **380**, 646–650 (1996).
13. van Gelder, C.W.G., Gunderson, S.I., Jansen, E.J.R., Boelens, W.C., Polycarpou-Schwarz, M. *et al. EMBO J.* **12**, 5191–5200 (1993).
14. Ibragimova, G.T. & Wade, R.C. *Biophys. J.* **74**, 2906–2911 (1998).
15. Pearson, N.D. & Prescott, C.D. *Chem. Biol.* **4**, 409–414 (1997)
16. Hermann, T. & Westhof, E. *Curr. Opin. Biotechnol.* **9**, 66–73 (1998).
17. Pearlman, D.A., Case, D.A., Caldwell, J.W., Ross, W.S., Cheatham, T.E. *et al. AMBER 4.1* (San Francisco, California; 1994).
18. Cornell, W.D., Cieplak, P., Bayly, C.I., Gould, I.R., Merz, K.M. *et al. J. Am. Chem. Soc.* **117**, 5179–5197 (1995).
19. Ryckaert, J.P., Ciccotti, G. & Berendsen, H.J.C. *J. Comput. Phys.* **23**, 327–336 (1977).
20. Berendsen, H.J.C., Postma, J.P.M., van Gunsteren, W.F., Dinola, A. & Haak, J.R. *J. Chem. Phys.* **81**, 3684–3690 (1984).
21. Darden, T.A., York, D. & Pedersen, L.G. *J. Chem. Phys.* **98**, 10089–10092 (1993).
22. Berendsen, H.J.C., Grigera, J.R. & Straatsma, T.P. *J. Phys. Chem.* **97**, 6269–6271 (1987).
23. Auffinger, P. & Beveridge, D.L. *Chem. Phys. Lett.* **234**, 413–415 (1995).
24. Dang, L.X., Pettitt, B.M. & Rossky, P.J. *J. Chem. Phys.* **96**, 4046–4047 (1992).

Stability of hairpin ribozyme tertiary structure is governed by the interdomain junction

Nils G. Walter[1], John M. Burke[1] and David P. Millar[2]

[1]Markey Center for Molecular Genetics, Department of Microbiology and Molecular Genetics, The University of Vermont, Burlington, Vermont 05405, USA. [2]Department of Molecular Biology (MB-19), The Scripps Research Institute, 10550 North Torrey Pines Road, La Jolla, California 92039, USA.

The equilibrium distributions of hairpin ribozyme conformational isomers have been examined by time-resolved fluorescence resonance energy transfer. Ribozymes partition between active (docked) and inactive (extended) conformers, characterized by unique interdomain distance distributions, which define differences in folding free energy. The active tertiary structure is stabilized both by specific interactions between the catalytic and the substrate-binding domains and by the structure of the intervening helical junction. Under physiological conditions, the docking equilibrium of the natural four-way junction dramatically favors the active conformer, while those of a three-way and the two-way junction used in gene therapy applications favor the inactive conformer.

The discovery of ribozymes[1,2] opened up new avenues for understanding structure-function relationships in RNA, since catalytic function reports the presence of an active tertiary structure. Recent advances in NMR spectroscopy and X-ray crystallography have revealed atomic details of RNA structure[3] but are largely unable to report conformational changes that are essential for biological function. Lower resolution methods such as fluorescence quenching assays[4], cross-linking studies[5], absorbance spectroscopy[6], electrophoretic mobility[7], hydroxyl radical footprinting[8], and differential probe hybridization[9] have recently begun to illuminate the complexity of RNA tertiary structure folding pathways.

A model system that is useful for studying RNA folding is the hairpin ribozyme, a reversible endoribonuclease that catalyzes cleavage and ligation reactions necessary for the rolling circle replication of a family of satellite RNAs associated with plant viruses[10]. Their proliferation involves autolysis of the replicated concatamer by a site-specific 2'-OH nucleophilic attack, and cyclization of the resulting RNA monomers. In the negative strand of tobacco ringspot virus satellite ((-)-sTRSV) RNA, the hairpin ribozyme is embedded within a four-way helical junction[11]. For biochemical studies *in vitro*, a minimal *trans*-acting ribozyme was engineered by deleting two of the four junction arms[11] (Fig. 1*a*). The resulting construct, containing a two-way junction, has been used for targeted RNA inactivation within mammalian cells, and is the basis for experimental strategies in human gene therapy of genetic and viral diseases[12].

No high-resolution data on the tertiary structure of the hairpin ribozyme are yet available[13]. Previous evidence has shown that catalytic activity requires a sharp bend about the hinge of the junction between the two domains A and B of the ribozyme–substrate complex (Fig. 1*a*), enabling a specific interdomain docking interaction[13]. Pre-steady state analysis has revealed biphasic kinetic behavior that results from formation of an alternative conformer of the ribozyme–substrate complex[14]; the two domains adopt an extended structure that lacks catalytic activity but can reversibly bind substrate[15]. Steady-